Validation of Loci-Stream for Autogenous Pressurization of Cryogenic Propellant Tank

Chintan S. Patel *
Qualis Corp (Jacobs Space Exploration Group), NASA Marshall Space Flight Center, Huntsville, AL

Brandon R. Williams †
NASA Marshall Space Flight Center, Huntsville, AL

Autogenous pressurization of cryogenic propellant tanks eliminates the need to have an additional pressurant tank on the space vehicle, which is highly advantageous due to reduced vehicle mass and design complexity. Autogenous pressurization therefore is one of the key technologies for deep space exploration and long-term space missions. The complex interaction of thermal gradients, turbulence and phase change near the interface make the problem a challenging one to model. Nodal analysis tools and reduced order models are unable to capture the necessary physics. 3-D CFD analyses are necessary to fully characterize autogenous pressurization. CFD analyses pose their own difficulties. The requisite CFD tool to tackle this problem need to be modular with the ability to incorporate various physics models, efficient, and computationally scalable for simulating flight size tanks. NASA MSFC's Loci-Stream CFD tool along with the VOF module is a great candidate to fit this mold. We demonstrate our modeling approach and validation of Loci-Stream for predicting autogenous pressurization of a flight scale propellant tank in order for the solver to serve as a reliable design and analysis tool for NASA's CFM application needs. Liquid hydrogen tank pressurization tests carried out at the MSFC test stand 300 facilities provide reliable validation data for this purpose. These tests were modeled using the Loci-Stream solver with a newly implemented two-phase sharp interface treatment. We show that our modeling approach and CFD solver predict the autogenous pressurization phenomena satisfactorily, and document challenging aspects of modeling this problem.

I. Nomenclature

A_{in}	=	Gas-liquid interface area
α	=	Thermal expansion coefficient
C_m	=	mass transfer coefficient (accommodation factor)
$_{cond}$	=	Subscript denotes condensation
dt	=	timestep
e	=	Internal energy
$_{evap}$	=	Subscript denotes evaporation
$\mathbf{G}$	=	gravitational force term in the momentum equation
$\mathbf{g}$	=	gravitational acceleration
$_g$	=	Subscript denotes gas
h	=	Enthalpy
$_{in}$	=	Subscript denotes gas-liquid interface
$_{i,j,k}$	=	Subscripts denote spatial co-ordinates in Einstein notation
k	=	Thermal conductivity
κ	=	Iso-thermal compressibility
$_l$	=	Subscript denotes liquid
$\dot{m}$	=	Phase change mass transfer (evaporation/condensation) rate

*Computational Fluid Dynamicist, Fluid Dynamics Branch (ER42), NASA MSFC
†Lead Aerospace Engineer - Fluid Mechanics, Fluid Dynamics Branch (ER42), NASA MSFC

^{n}	=	Superscript denotes interface normal component
p	=	fluid pressure
Φ	=	Heat dissipation through shear stress in total energy equation
R_g	=	Specific gas constant
ρ	=	density of fluid
$_{sat}$	=	Subscript denotes saturation condition
T	=	Static temperature
t	=	Time
^{t}	=	Superscript denotes interface tangential component
τ	=	Shear stress tensor
$\mathbf{u}$	=	fluid velocity
V	=	Volume

Note: All vectors/tensors, except when using Einstein notation, are represented with **bold** font.

II. Introduction

NASA's near-future long-term space missions necessitate advancements in cryogenic fluid management (CFM), which includes safe, low cost, and reliable long-term propellant storage. Consequently, NASA STMD (Space Technology Mission Directorate) has established the CFM Portfolio Project to improve CFM technologies for upcoming missions.

In addition to advanced hardware development and demonstration, there is a need for accurate modeling of cryogenic system behavior to support rapid, reliable, and low-cost spacecraft design and operation. As part of the CFM modeling portfolio, the Propulsion Engineering Fluid Dynamics branch at NASA Marshall Space Flight Center (MSFC) has been tasked with assessing and improving computational tools used to support future and current flight projects such as Human Lander System and Commercial Lunar Payload Services. We are engaged in improving and validating multiphase models in the Loci-STREAM computational fluid dynamics (CFD) code to predict various CFM phenomena.

While cryogens are desirable fuel choice due to high specific impulse, long-term storage and operation is challenging. Propellant must be supplied to the engine in an operating pressure range for safe operations. Traditionally, spacecraft use an inert pressurant gas (nitrogen, helium, etc.) to maintain operational pressure during engine firing. Long duration space flight missions have stringent design requirements for propulsion storage and use. Carrying additional weight of a separate pressurant tank to pressurize the main propellant tanks is not economical. A separate tank also adds design complexities with additional plumbing. A fixed storage of inert gas pressurant can also be a limiting factor once in-space propellant refueling or lunar propellant production is available to extend flight duration.

Autogenous pressurization is a promising solution to these problems. Some of the cryogenic liquid propellant is tapped, evaporated, and reintroduced in the tank ullage to increase tank pressure. The need to carry a separate pressurant tank is therefore eliminated and the flight vehicle is structurally more robust and less complex. The simplified system offers higher reliability with fewer components. The fuel and the oxidizers are completely isolated, and there is no contamination of propellant from pressurant gas.[1]

When a tank is autogenously pressurized, the ullage gas near the interface can readily condense under the increasing ullage pressure. The dynamics of velocities, turbulence, thermal gradients, and saturation condition at the interface determine the re-condensation of ullage gas. Understanding theses dynamics at the gas-liquid interface is challenging. These dynamics drive the requisite design heat flow rates, mass flow rate, and pressurization time as well as frequency required to obtain and maintain a design pressure for an engine firing. A good understanding of these dynamics is demonstrated when we can capture salient features of the experiment through modeling. The heat fluxes encountered at the interface are much higher than during self-pressurization and require extra care in modeling. Specifically for liquid hydrogen, due to the high latent heat of vaporization, the heat exchange at the interface can be significant and the capture of thermal gradients can be challenging.

In this paper, we show validation of NASA MSFC's Loci-STREAM CFD solver for predicting autogenous pressurization using experimental ground tests. The principal aim of the work documented in this paper is to validate the Loci-Stream CFD tool and our modeling technique for CFM and propellant tank dynamics applications and discuss challenging aspects of modeling. In the following sections, the experimental set-up, governing equations, newly implemented Loci-Stream two phase sharp interface CFD model for gas-liquid interface, mass transfer model, and finally a comparison of the simulation results and experimental data are presented.

III. Test Description

The evolvable Cryogenics (eCRYO) project was set-up to develop and advance state of the art, in-space cryogenic propellant management technologies with a focus on long duration missions. Under the eCRYO project, the Integrated Vehicle Fluids (IVF) task was set up among other objectives to manage propellant boil-off. This task repurposed the CPST (Cryogenic Propellant Storage and Transfer) EDU (Engineering Design Unit) tank as the IVF-1000 tank (shown in Figure 1). EDU tank was originally designed to develop manufacturing techniques and reduce risk for future CFM applications. Emphasis was put on flight-like tank and peripherals design.

Several tests were carried out under IVF phase A testing using this IVF-1000 tank (sometimes still referred to as CPST EDU tank or simply EDU tank) to characterize various aspects of cryogenic tank dynamics using liquid nitrogen, hydrogen, and helium. On day 3 of this testing, an autogenous pressurization test was conducted with low diffuser massflow rate, specifically for generating a dataset for validation of nodal computational modeling and analysis tools.

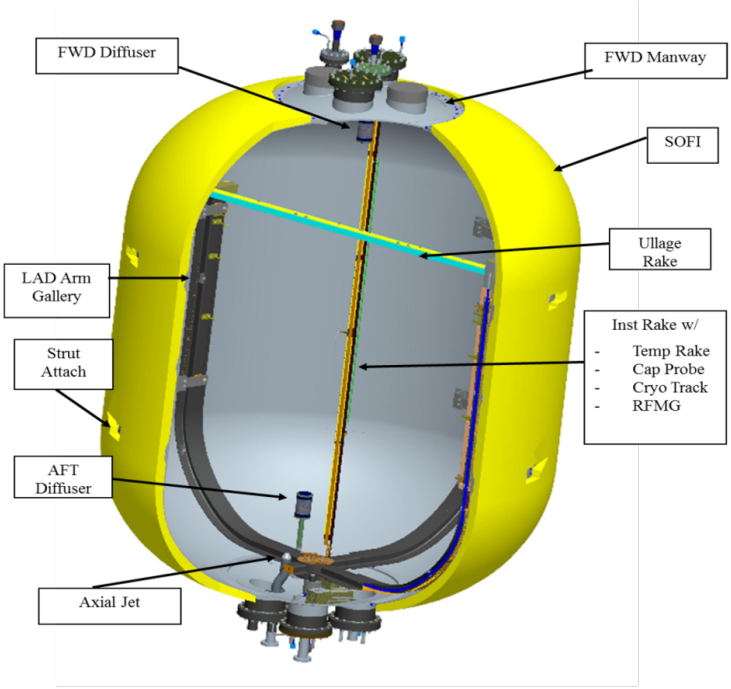

Fig. 1 CAD model of the IVF-1000 Tank with the Internals

A. Testing Facilities

The cylindrical double-domed tank is constructed with 2 mm thick 2219 aluminum and has an internal volume of 4.367 m^3. The tank cylinder has a radius of 0.852 m and height of 2.334 m, and the half oblate spheroids have a minor radius of 0.615 m. The tank is insulated with Spray-On Foam Insulation (SOFI) as well as Multi-layer Insulation (MLI) for insulation in vacuum conditions. The tank was mounted on a stand with struts and housed in vacuum chamber at NASA MSFC test stand 300. A series of pressure and temperature sensors (see Figure 2) were located on horizontal and vertical rakes inside the tank, on the diffuser inlet, the tank wall, and the MLI layers.

B. Experimental Procedure

For this autogenous pressurization modeling test, the tank was filled with liquid hydrogen (LH2), vented at atmospheric pressure to achieve a saturated gas-liquid interface and then locked-up at 90% fill volume. Temperature probe data from ullage, diffuser and suggest uniform initial temperature was achieved. All drain valves remained closed throughout this test. Room temperature gaseous hydrogen (GH2) pressurant at 297 K was introduced into the ullage through the diffuser for approximately 100 seconds. The measured diffuser mass flow history is shown in Figure 3 along with the corresponding ullage pressure.

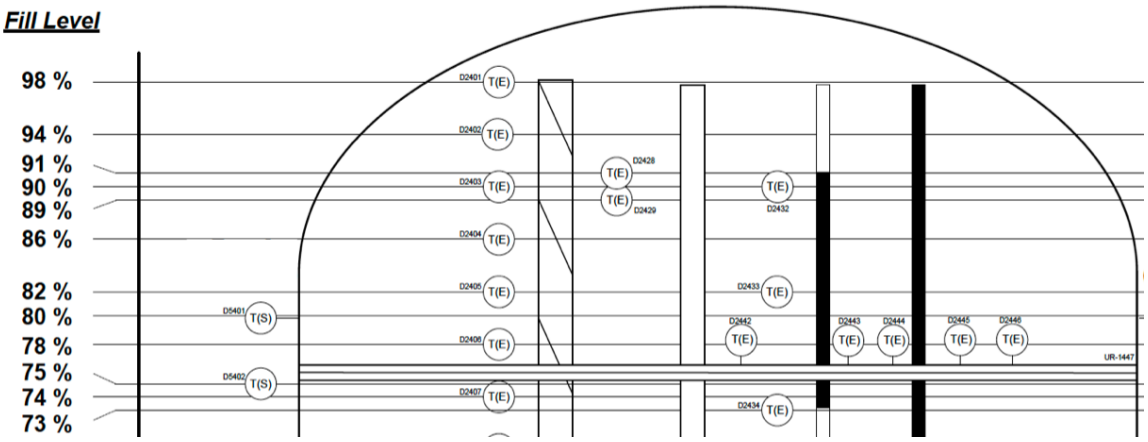

(a) Fluid Sensors inside the Tank

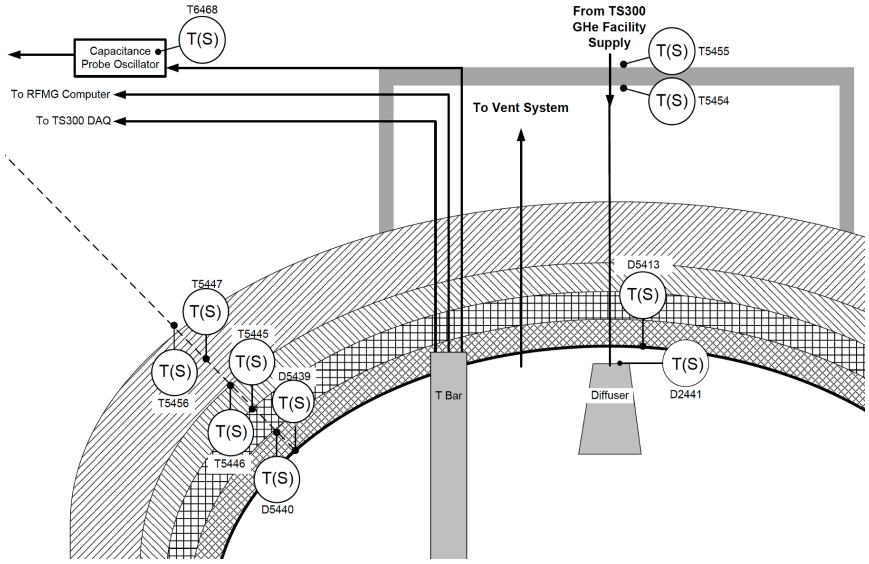

(b) Solid Wall Sensors on Tank Structure

Fill Level (%)	Tank Station (in)	Instrumentation ID		
		Temperature Rake	Cryo Tracker	RFMG
98	85.2	D2401		
94	80.2	D2402		
91	77.3	D2428		
90	76.4	D2403	D2432	
89	75.6	D2429		
86	73.1	D2404		
82	70.0	D2405	D2433	
78	67.0	D2406		

(c) Locations of Fluid Sensors (Distances are measured from tank bottom)

Fig. 2 Temperature and Pressure Sensors

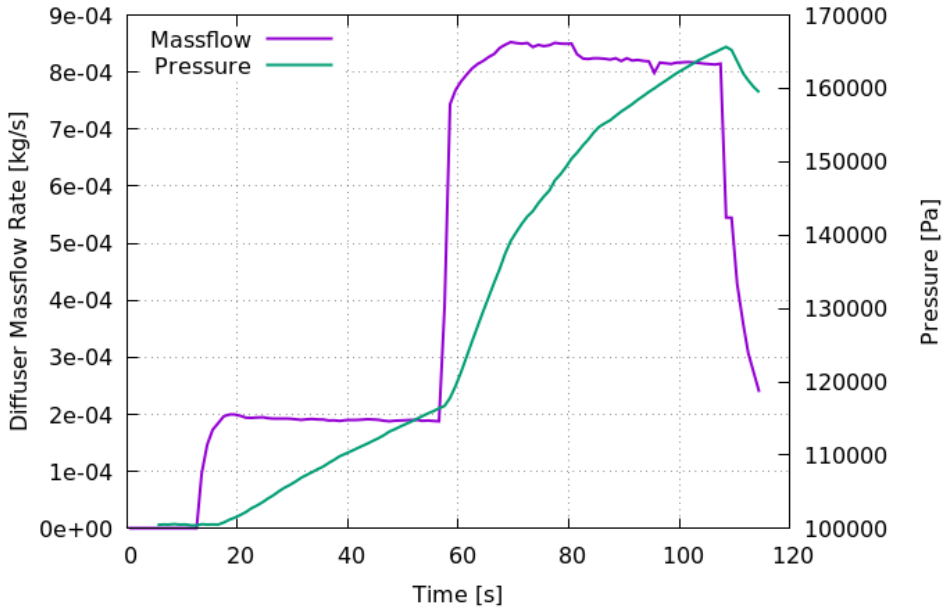

Fig. 3 Diffuser Massflow and Corresponding Tank Pressure

IV. Computational Model

A. Governing Equations

The governing equations for mass, momentum, and energy conservation are given in the Equation 1, 2 and 3. These equations are for single-phase fluids and implemented in the Loci-Stream code [2, 3]. The two-phase sharp interface method is described in the subsection *Two Phase Sharp Interface Model*. Here, we merely note that a single set of governing equations are solved for both phases and the gas-liquid interface is treated as a boundary.

$$\frac{\partial \rho}{\partial t} + \frac{\partial \rho u_j}{\partial x_j} = 0 \tag{1}$$

$$\frac{\partial \rho u_i}{\partial t} + \frac{\partial \rho u_j u_i}{\partial x_j} = \frac{\partial p}{\partial x_i} + \frac{\partial \tau_{ij}}{\partial x_j} + \mathbf{G} \tag{2}$$

$$\rho c_p \frac{DT}{Dt} = \alpha_l T \frac{Dp}{Dt} + \frac{\partial}{\partial x_i}(k \frac{\partial T}{\partial x_i}) + \Phi \tag{3}$$

The Boussinesq approximation is invoked in the momentum equation for the buoyancy source term. The liquid density is assumed to be constant except for calculating the buoyancy force, where the liquid density is considered a linear function of temperature in the gravity term. Equation 4 defines the contribution to the body force in momentum equation, where ρ_{ref} is liquid density at the reference temperature T_{ref}.

$$\mathbf{G} = -\alpha_l \, \rho_{ref} \, (T - T_{ref}) \, \mathbf{g} \tag{4}$$

B. Energy Conservation

The energy equation conserves total energy of the system as described in Equation 5. In a previous study of constant density problems, the internal energy form, was used [4, 5]. Barsi and Kassemi [4, 5] presented a comprehensive review of the various constant density models, among which the CFD models were able to provide detailed simulations of tank pressure evolution for the current K-site experiments, together with two dimensional (2-D) and or 3-D depictions of the temperature and velocity fields. Using the internal energy form, Barsi and Kassemi [4] showed favorable agreements with the experimentally measured pressure histories. In this study, however, the conservation is imposed by an enthalpy-based formulation (Equation 3).

$$\rho \frac{De}{Dt} = \nabla(k\nabla T) - p\,\nabla \cdot \mathbf{u} + \Phi \tag{5}$$

$$de = \left(\frac{\partial e}{\partial T}\right)_{\rho} dT + \left(\frac{\partial e}{\partial \rho}\right)_{T} d\rho = c_v dT + \frac{1}{\rho^2}\left(p - \frac{\alpha T}{\kappa}\right) d\rho \tag{6}$$

The change in internal energy is defined by the thermodynamic relation in Equation 6. For some propellant (such as liquid hydrogen), the density variation term in Equation 6 has significant contribution, so this term needs to be included in Equation 5 for accurate modeling. However, the geometrical reconstruction and backward projection of the VOF formulation are purely based on the assumption of conservation of liquid volume. In order to conserve total liquid mass, one must assume the liquid density to be constant. Thus, a physics-accurate internal energy formulation cannot be easily implemented alongside the VOF formulation.

The aforementioned problem is solved by representing the total energy conservation in a different thermodynamic state variable, enthalpy. Internal energy and enthalpy are related in Equation 7. Unlike the internal energy variation (Equation 6), the enthalpy variation (Equation 8) does not depend on density, and therefore this formulation is consistent with the VOF method. Substitution of Equation 7 in Equation 5 leads to the enthalpy-based total energy conservation (Equation 9). Finally, Equation 8 is used to obtain the conservation equation for the primitive solved variable, i.e., temperature (Equation 3). Note that regardless of the representative form, the property being conserved is total energy, which for our purpose is summation of internal energy and kinetic energy.

$$e = h - \frac{p}{\rho} \tag{7}$$

$$dh = \left(\frac{\partial h}{\partial T}\right)_{p} dT + \left(\frac{\partial h}{\partial p}\right)_{T} dp = c_p dT + \frac{1}{\rho}(1 - \alpha T) dp \tag{8}$$

$$\rho \frac{Dh}{Dt} = \frac{Dp}{Dt} + \nabla(k\nabla T) + \Phi \tag{9}$$

C. Phase Change Mass Transfer

The mass transfer rate due to phase change between the gas and liquid phases ($\dot{m}$) is based on the model described by Hertz-Knudsen-Schrage (HKS) (Equation 10) [6], where all quantities are represented in SI units. The HKS equation is based on statistical mechanics and thermodynamics states of the phases, and heat transfer is not considered. The HKS equation works well in near-equilibrium conditions.

Mathematically at saturation condition and at equilibrium, $C_{evap} = C_{cond}$ must be true. While these assumptions may not be satisfied with a large temperature gradient found in the autogenous pressurization problems, because the coefficients are empirically unknown, we invoke these assumptions for the simplicity of the model. With these assumptions, we write simplified HKS equation (Equation 11), which is from here referred to as HKS equation for brevity. Note that the accommodation factor ($0 < C_m \leq 1$) must be supplied, and its choice is discussed in the *Effect of Accommodation Factor* section below.

$$\dot{m} = \sqrt{\frac{1}{2\pi R_g}} \left(C_{evap} \frac{p_{sat}(T_l)}{\sqrt{T_l}} - C_{cond} \frac{p_g}{\sqrt{T_g}}\right) A_{in} \tag{10}$$

$$\dot{m} = C_m \sqrt{\frac{1}{2\pi R_g T_{in}}} \left(p_{sat} - p_g\right) A_{in} \tag{11}$$

Saturation pressure is obtained using the Antoine equation (Equation 12), where the constants for a given fluid are sourced from NIST thermodynamic data [7].

$$log_{10}\, p_{sat} = a - \frac{b}{c + T_{sat}} \tag{12}$$

D. Two Phase Sharp Interface Model

While VOF is a high-fidelity model for capturing the evolution of a gas-liquid interface, the accuracy and generality come with a higher computational cost compared with other methods. For the long duration self-pressurization scenarios described above, that computational cost may become a significant disadvantage. Because the interface is static, other methods where the gas and liquid domains are simulated in a segregated but coupled fashion are also possible.

A lumped gas sharp interface model was developed into Loci-Stream previously to overcome timestep size and stability limitations of VOF for low momentum and quiescent-interface flows [8]. This method was well-suited for self-pressurization problem in CFM due to largely quiescent ullage and the dynamic primarily being driven by liquid dynamics. While that method works very well for the problem, the obvious disadvantage is in foregoing understanding of ullage dynamics when they are important. Therefore, we generalize the method here to two phase sharp interface model. While self-pressurization generally does not require resolution of ullage dynamics, this method is essential for modeling many CFM problem, for example, autogenous pressurization. A brief description of the model follows.

The interface between the gas and liquid is assumed to be unperturbed. But both gas and liquid are explicitly modeled with 3-D CFD. Boundary conditions on each side of the interface must be supplied. Interface tangential velocities are same on both sides of the interface (Equation 13). Additionally, the interface tangential shear stress is also equal across the interface (Equation 14). Interface normal velocity is assumed to be zero - even when phase change occurs. This is justified because the phase change mass transfer and corresponding velocities are very small and our testing with a momentum source term found no stability improvement.

$$u^t_{in,l} = u^t_{in,g} \tag{13}$$

$$\tau^t_{in,l} = \tau^t_{in,g} \tag{14}$$

$$u^n_{in,l} = u^n_{in,g} = 0 \tag{15}$$

Phase change is modeled using a mass source term. Two models are implemented to model heat transfer and mass transfer across the interface, as described by Kassemi, et al [9]

1. Balance Method

In this method, the ullage gas in contact with the sharp interface is assumed to be at equilibrium condition (i.e., saturated at all times). Then the temperature of the gas side of the interface can be calculated using saturation condition at current ullage pressure. Clausius-Clapeyron and Antoine equations are the most often used relationships between saturation temperature and pressure. Both methods are implemented. Antoine equation (Equation 12) which superior in closely approximating saturation curve is chosen for our simulations.

The "balance" refers to thermal balance at the interface. It is assumed that the interface is always in thermal equilibrium, i.e., the heat flux to the interface from the liquid is equal to heat flux to the interface from gas plus the flux from the latent heat of evaporation (Equation 16). This equilibrium yields phase change mass transfer rate, $\dot{m}$.

$$\dot{m}L = Q_l - Q_g \tag{16}$$

2. Kinetics - Balance Iterative Method

This method combines the kinetic relationship for phase change mass transfer rate provided by the HKS (Equation 11) and thermal balance at the interface (Equation 16). We solve these equations iteratively using secant method to obtain the interface temperature, T_i. Here, the interface is not assumed to be saturated.

The sharp interface approach provides all the benefits of the lumped gas liquid CFD approach [8]. First, the use of computationally expensive VOF advection and geometric reconstruction of the VOF method is circumvented. Second, the stringent Courant number stability constraint for explicit timestepping in the VOF method is also avoided. Since Loci-Stream is an implicit solver in time, an order of magnitude or even higher timestep can be used with sharp interface method. Third, the problem of small computational instabilities at the gas-liquid interface inherently present in the VOF method on any practical non-orthogonal mesh is also resolved, allowing careful resolution of thermal gradients and velocity profiles with mesh refinement that is impractical for the VOF method.

E. Turbulence Modeling for Two Phase Interface

Turbulence modeling at the two-phase interface with two-equation RANS models is tricky. Menter (1994), Wilcox (1998) and others have shown that eddy viscosity based turbulence models generate non-physically high turbulence near the interface compared to the experimental observations [10]. Modifications must be made to two equation model in this region. The most common approach is promulgated by Egorov [11], in which ω-equation is modified to a more wall-like treatment to damp the turbulence. This approach has shown to be effective in wide-ranging applications [12]. The intuition for the method is that when high density ratio fluids are interacting, the lower density fluid essentially "sees" the higher density fluid as a wall. Yet the method is applied to both phases symmetrically and an asymmetric approach where the heavier fluid sees the lighter fluid as a slip-wall for purpose of turbulence modeling may be more appropriate [10]. We note that a high value of the damping factor in Egorov's method is recommended but the clear consensus for these values does not exist, and the choice is mesh dependent [10].

Here, we forgo the complexity and some disadvantages of the Egorov method and retain the insight and advantages with a simpler model. We implement two turbulence treatments at the interface that bound the expected behaviors. In the first method, the interface is treated as wall-like for turbulence boundary conditions. In the second method, the interface is treated as slip-wall-like for turbulence boundary conditions where boundary turbulence is simply extrapolated from the nearest non-boundary cell. For the ullage gas, we always employ the wall-like turbulence treatment. For the much heavier liquid phase, either one of the techniques may be appropriate depending on the physics. We end this section by noting that the symmetric wall-like turbulence treatment is akin to using Egorov's method with a very high damping factor.

V. Modeling

A. Set-up

The most salient features of problem are to be captured with CFD. Modeling is rendered as simple as possible while ensuring retention of all important physics. This approach saves significant computational time and enables exploration of validation sensitivities to confidently apply the solver and our modeling approach to wide scale/range of CFM problems. All tank internals are insignificant to the problem and are removed with the exception of the forward diffuser. A design, in which the diffuser is not modeled, and inlet to the ullage is represented with a simple stub/slot was considered. We found that this simplified approach does not capture the heat transfer from the hot 297 K inlet flow to the diffuser wall initially at 20 K, which is crucial to predicting tank pressurization. The diffuser solid walls and flow through the diffuser must be modeled to accurately capture the heat transfer between them, which results in a nearly 50 K temperature drop of the inlet flow before the hydrogen enters the ullage.

An axisymmetric flow assumption is made as no important circumferential flow- and thermal- dynamics is expected. The computational domain contains 1° sectors of the press line, forward diffuser, tank fluid and tank walls. The diffuser in the test article contains 48 exit holes to the ullage. These non-axisymmetric holes were simplified as three axisymmetric slots with equivalent exit area. The simplification to the cylindrical slots segments the diffuser and separates the bottom part from the top. So, the location of the slots was chosen to be away from the press line on the diffuser to ensure conduction through the diffuser walls, the heat transfer with the gas, and the heat retention by the diffuser walls are predicted as closely as possible with the axisymmetric model.

The tank walls are also modeled using conjugate heat transfer analysis. We conducted analyses with and without the inclusion of the solid tank walls and found that the heat transfer between the cryogen and the cold tank wall was very important to predict pressurization, because they retain a non-trivial fraction of the thermal energy input from the diffuser inflow.

The measurements across the 40 MLI temperature probes show that the tank is well-insulated and the heat transfer at the external tank wall is infinitesimal. The tank aluminum external wall is considered adiabatic.

B. Mesh

The computational mesh must be able to capture the important features of the high-speed diffuser flow, low velocity ullage flow with convection and heat transfer between ullage gas at cryogenic temperatures and pressurant gas at room temperature, and the sharp thermal gradient at the gas-liquid interface. Unstructured hexahedral meshes are used for this validation for their computational efficiency. Several meshes with varying resolution in the diffuser, ullage and interface regions were constructed and tested. A representative sample is presented in the Figure 5. To accurately calculate the

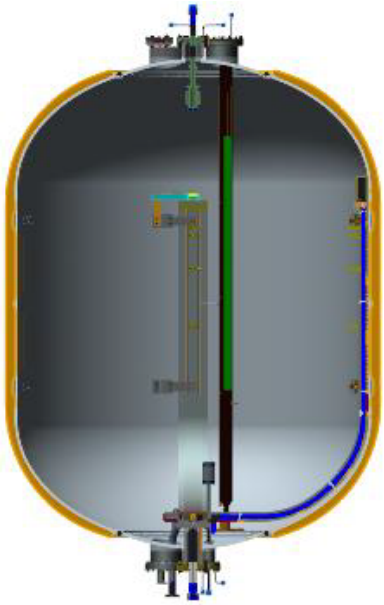

(a) Tank CAD Model Cross-section [13]

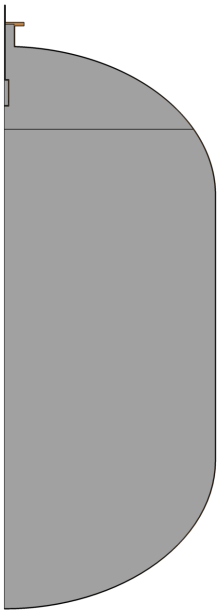

(b) Simplified Domain for Modeling

Fig. 4 Tank Model with and without Tank Internals

heat transfer between the wall and the fluid, full integration to the wall approach was used. The boundary first cell height was varied between 1×10^{-4} m and 5×10^{-5} m. The nominal cell edge length in the ullage varies between 2.5 mm and 7 mm. The interface first cell height was between 1×10^{-4} m and 1×10^{-6} m.

The coarsest mesh (Figure 5a) has 25,480 cells on the axisymmetric plane, which is an equivalent cell count of 9.2 million cells for a full 3-D model. Successive refinement yields equivalent cell counts of 18.8 million (Figure 5b), and 40.6 million (Figure 5c). The baseline mesh was further refined at the interface to achieve a refined-interface mesh with 22.3 million cells. Solution sensitivity to the mesh is presented in the *Mesh Resolution Sensitivity* section.

C. Initial and Boundary Conditions

Temperature probe data show nearly uniform temperature across the liquid and the ullage at the onset of the experiment. Therefore, a uniform initial temperature initial condition was applied. This temperature corresponds to the saturation condition for hydrogen at the atmosphere pressure. Time-varying massflow and temperatures were measured during the test and were prescribed at the diffuser inlet. A time-varying mass-flow boundary condition was implemented at the diffuser inlet by supplying an input file that specifies GH2 mass-flow rate and temperature.

An adiabatic wall condition was prescribed at the external tank wall surface as discussed in the *Set-up* section. As the inlet is expected to have "medium" turbulence, turbulence intensity of 5% with eddy viscosity ratio of 1000 were prescribed. Several simulation tests were carried out to ascertain impact of initial turbulence and diffuser inlet turbulence. We found the pressurization predictions were insensitive to a wide range of the turbulence conditions. A symmetry boundary condition was applied on the sector planes.

D. Fluid Properties

Fluid and material properties were evaluated from the current National Institute of Standards and Technology (NIST) databases [7]. The liquid hydrogen is assumed to be a Boussinesq fluid to model buoyancy, while the ullage is modeled as a compressible ideal gas. We note that the ideal gas assumption deviates about 12% from the real gas behavior [13]. Since there is dramatic variation in ullage temperature due to the introduction of room temperature gaseous hydrogen pressurant, temperature-dependent vapor phase properties were modeled. The specific heat of the gas was defined with two piecewise fourth order polynomials. The transport properties – conductivity and viscosity – from the NIST database were fitted to Sutherland's law.

The solids are modeled with aluminum 2219 thermal properties at the appropriate temperatures. Temperature

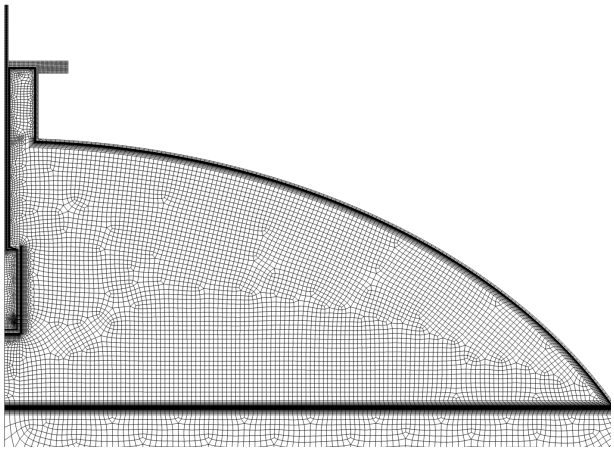

(a) Coarse Mesh - Ullage and Diffuser

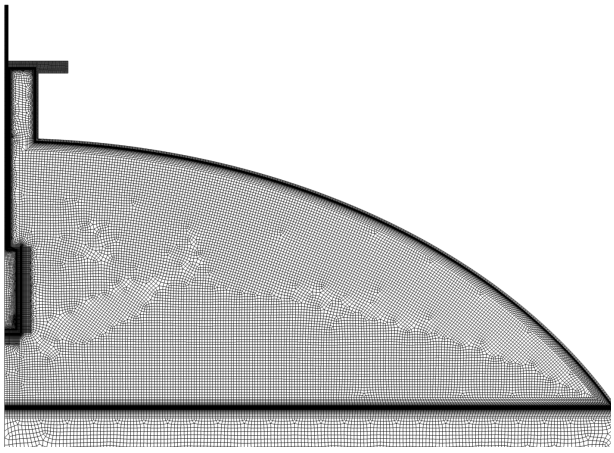

(b) Baseline Mesh - Ullage and Diffuser

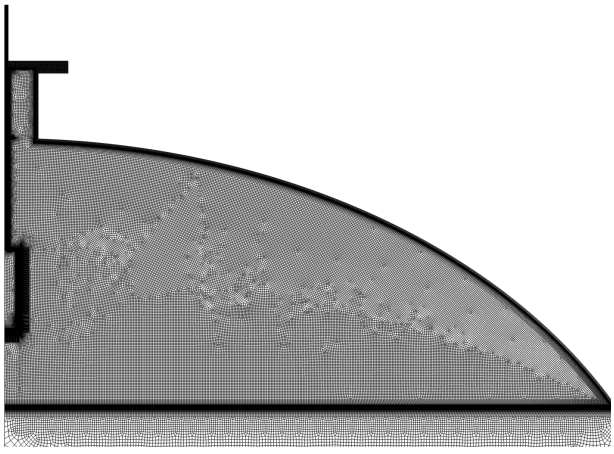

(c) Refined Mesh - Ullage and Diffuser

Fig. 5 Mesh resolutions used for validation and verification

dependent solid properties are not supported at present. These properties impact the pressurization rate by means of modulating heat conduction and retention in the tank walls and diffuser, so within this limitation we must carefully select the properties at the operating temperatures which capture the essence of the heat transfer between the fluid and

the solids. The diffuser, which is in contact with the hottest flow, therefore used aluminum 2219 properties [14] at a higher temperature than the tank which the experimental data show to remain at relatively cooler temperature throughout the experiment.

The liquid (Table 1), gas (Table 2), diffuser (Table 3) and tank (Table 4) properties are listed in the tables below.

Parameters	Description	Value
ρ_l	Liquid density	$71.0386\,\mathrm{kg/m^3}$
c_{pl}	Liquid specific heat at constant pressure	$9680.24\,\mathrm{J/Kg/K}$
k_l	Liquid thermal conductivity	$0.103\,681\,\mathrm{W/m/K}$
μ_l	Liquid dynamic viscosity	$1.367\,69 \times 10^{-5}\,\mathrm{kg/m/s}$
α_l	Liquid volume expansion coefficient	$0.0168\,\mathrm{K}$
L	Latent heat	$445.800 \times 10^3\,\mathrm{J/kg}$
σ	Surface tension	$0.001\,939\,62\,\mathrm{N/m}$

Table 1 Liquid Hydrogen Thermodynamic Properties

Parameters	Description	Value
ρ	Density	Ideal gas
c_{pg}	Specific heat at constant pressure	Function of temperature
k_g	Thermal conductivity	Function of temperature
μ_g	Liquid dynamic viscosity	Function of temperature

Table 2 Gaseous Hydrogen Thermodynamic Properties

Parameters	Description	Value
ρ	Density	$2840.0\,\mathrm{kg/m^3}$
c_p	Specific heat at constant pressure	$780.0\,\mathrm{J/Kg/K}$
k	Thermal conductivity	$115.0\,\mathrm{W/m/K}$

Table 3 Aluminum 2219 Thermodynamic Properties at 150 K for Diffuser

Parameters	Description	Value
ρ	Density	$2840.0\,\mathrm{kg/m^3}$
c_p	Specific heat at constant pressure	$550.0\,\mathrm{J/Kg/K}$
k	Thermal conductivity	$71.0\,\mathrm{W/m/K}$

Table 4 Aluminum 2219 Thermodynamic Properties at 50 K for Tank Wall

E. Flow Regime

The high velocity diffuser inlet flow is expected to have moderate turbulence. After the diffuser flow enters the ullage, the velocities are quite low. Even at these low velocities, free shear, high temperature gradients and consequent convective currents make the ullage flow turbulent. Therefore, the turbulence must be modeled. Indeed, we found that a well-resolved laminar solution fails to predict heat transfer with the tank walls and within the ullage and over-predicts the interfacial temperature and ullage pressurization (see Figure 12 and section *Flow Regime and Turbulence Model*

Sensitivity where more details are discussed). Here, we note that for turbulence modeling, we focused on two equation RANS models. Menter's k-ω shear stress transport model (referred to as k-ω-SST or simply SST) was evaluated. The k-ω SST with Improved Delayed Detached Eddy Simulation (IDDES) - a hybrid RANS-LES approach, and a laminar model were also simulated for comparison.

F. Simulation Details

Time integration is computed implicitly with the second-order backward Euler method. A second order upwind scheme is used for spatial discretization. Yet when compared to the first order schemes, they were found to have little impact on the solution. For baseline mesh, $1e-2s$ timestep was used. Requisite timestep size and grid resolution sensitivity is presented in the forthcoming sections.

The Antoine equation (Equation 12) is used for the calculation of the saturation condition with coefficient $a = 3.168083$, $b = 78.059891$, $c = 4.315199$. The kinetics - balance iterative method was used for phase change, which provides more modeling flexibility than the balance method because it does not assume equilibrium condition at the gas-liquid interface. The accommodation factor coefficient in the phase change model is set to 1.0. Sensitivity to the accommodation factor used in the phase change model (Equation 11) is also presented in the forthcoming sections.

The Loci-Stream solid heat module is used for conjugate heat transfer analysis. A tight fit between the diffuser tube and tank wall was assumed and a small thermal contact resistance of $1e-16$ was supplied for their contact surface.

VI. Results

A well-reasoned modeling approach must come together with a capable solver and low conservation errors to produce a robust model that does not require any tuning parameters for validation. Such a model can be then extended to similar classes of problems with confidence.

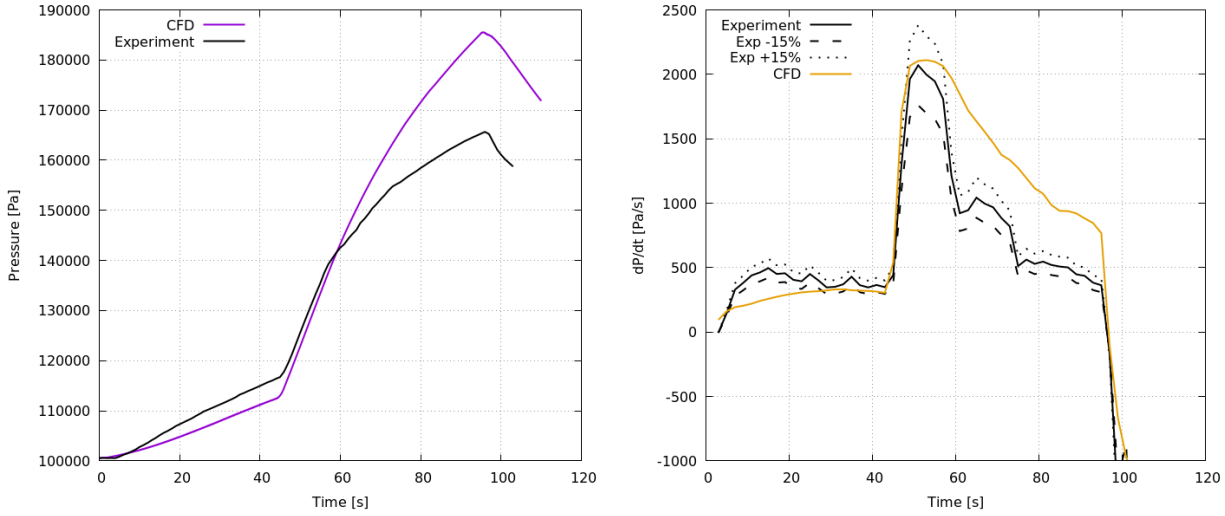

(a) Pressure vs Time **(b) Pressurization Rate vs Time**

Fig. 6 Pressure and Pressurization Rate Compared with the Experiment

Using the baseline mesh (Figure 5b) and the solution parameters described above, Loci-Stream was able to predict tank pressurization with satisfactory accuracy (Figure 6a). The pressurization rate is also captured satisfactorily (Figure 6b). Notable flow and thermal features are discussed below along with the problem sensitivities. The deviations from the experiments are also discussed, as the model limitations must be well understood and if deemed critical, addressed for reliable future applications.

We note here that the pressurization rate is over 1000 times higher than the rates encountered in self-pressurization problems. The high pressurization rate changes the saturation condition at the interface rapidly and causes rapid condensation of the gaseous hydrogen. The latent heat of hydrogen is quite high ($L = 445.8 \times 10^3$ J/kg). These factors result in a high temperature gradient on the ullage side of the interface, which must be captured with sufficient mesh

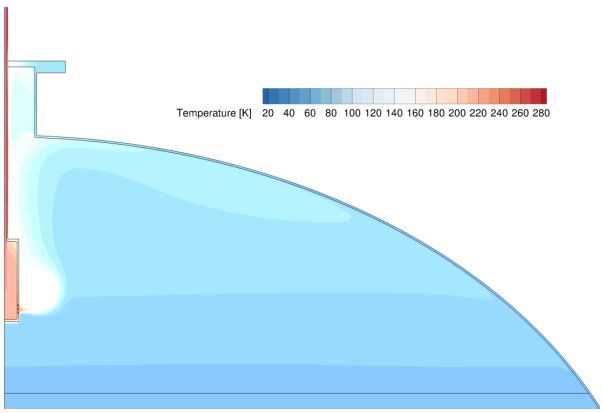

(a) Temperature

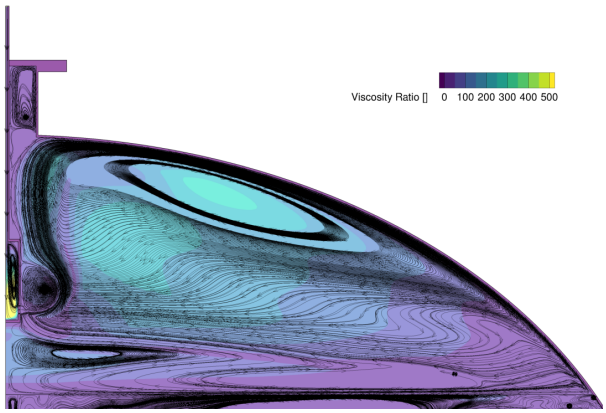

(b) Turbulence Viscosity Ratio with Streamlines

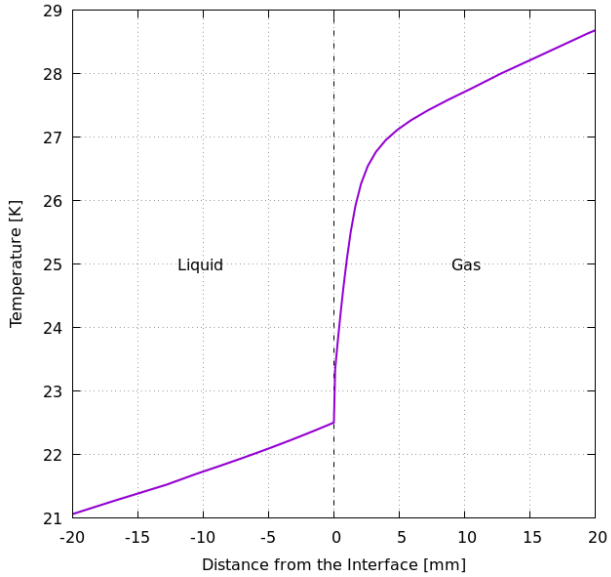

(c) Thermal Gradient at the Interface

Fig. 7 Field Variables and Interface Thermal Gradient at 90 seconds

resolution to predict interface temperature, which in turn guides the ullage pressure. The sharp thermal gradient resolved through the CFD is shown in the Figure 7c. We found that a 1×10^{-4} m first cell height at the interface was sufficient to capture the gradient.

The mass transfer involved with the high condensation rates is carefully modeled. Our solver is stable even at high accommodation factors and we are able to model the experiment with accommodation factor of 1. Figure 9 demonstrate the high condensation rates (by convention, the negative values denote condensation). Because the incoming hot diffuser flow has lower density than the cold hydrogen being condensed at the interface under an isochoric process, the condensation rate is as much as 3.5 times higher than the diffuser inflow rate (Figure 9b). Consequently, the mass of the gaseous hydrogen in the ullage at the end of autogenous pressurization is lower than the mass at the onset.

The pressurization rate (Figure 6b) compares very well till 60 s, after which the CFD prediction remains slightly higher than the experiment. The modeled ideal gas equation of state deviates 9 to 15% throughout the experiment from the real gas behavior (sourced from NIST [7]) at the saturation temperature, i.e., the interface density and the volumetric heat capacity ρc_p of the interfacial gas is under-predicted by 9-15% when using the ideal gas relation, which results in higher temperature increase for a given heat flux. A real gas model is therefore expected to reduce pressurization by the same 9-15% magnitude throughout the experiment. About 50% of the difference between the experiment and the model pressure is attributable to the ideal gas assumption. Moreover, the latent of vaporization is assumed constant due

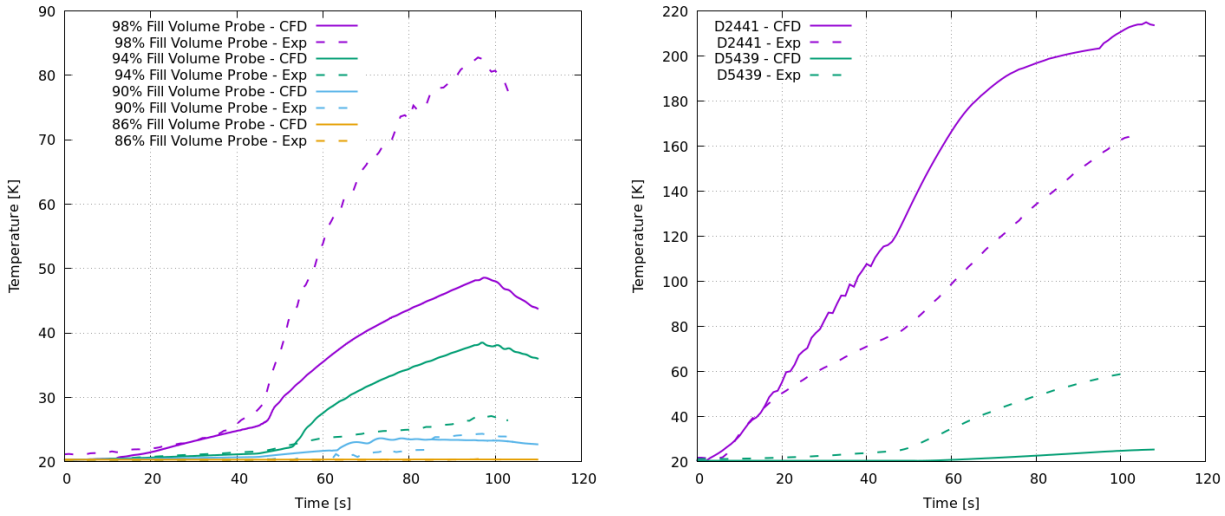

(a) Fluid Probes **(b) Ullage Probes**

Fig. 8 Probe Temperatures vs Time

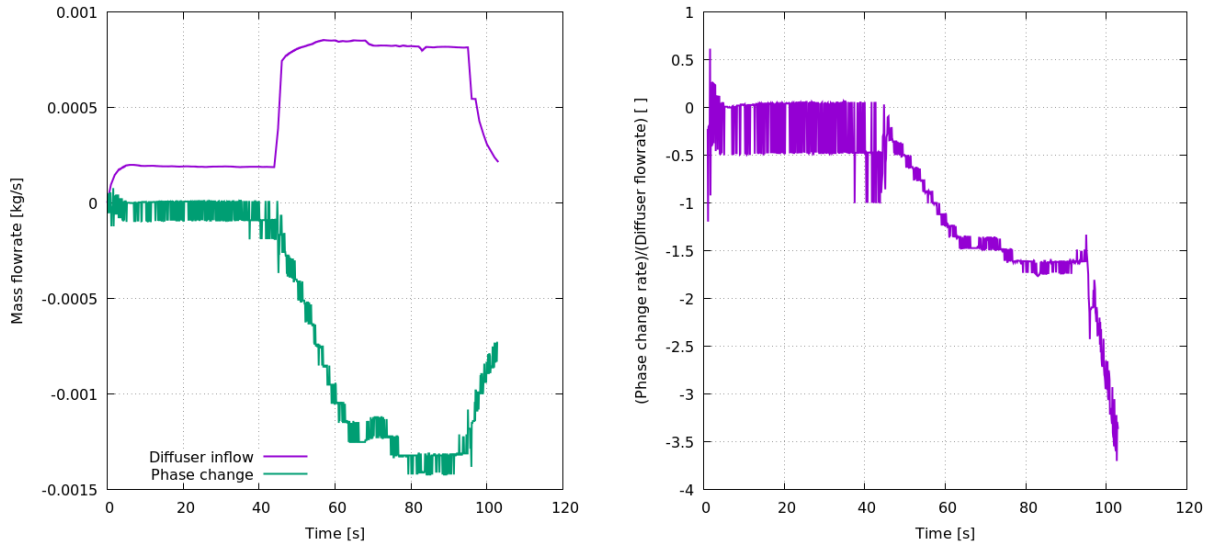

(a) Massflow Rates **(b) Ratio of Massflow Rates**

Fig. 9 Phase Change Mass Transfer Rate Comparison with Diffuser Flow Rate

to the current solver implementation but actually reduces 2.5% at the end of the test compared to the start of the test. Assuming equilibrium condition heat transfer at the interface, modeling variable latent heat is expected to modestly increase condensation as experiment progressed, which may also slightly improve the prediction of pressurization rate.

A comparison of temperature probe data (see locations in Figure 2), while capturing the trends well, shows a less than satisfactory quantitative agreement (Figure 8) with the experiment across the tank walls and tank fluids. The temperatures predicted well under the lower diffuser massflow ($t < 44$ s). But under the higher diffuser massflow, the fluid temperature at the 98% fill volume probe is under-predicted while it is over-predicted at 94% fill volume probe, i.e., the thermal stratification of the ullage is diminished. The higher temperature prediction just above the gas interface due to the over-prediction of turbulence conductivity in the freestream region may also modestly add to the over-prediction of the temperature in the interface region due to ideal gas assumption. In our experience, the two equation turbulence models have difficulty maintaining thermal gradients in the ullage due to this over-prediction of turbulence conductivity

- even when much lower temperature gradient than those encountered in this problem exist. This behavior has also been observed by others [9] [15]. This over-prediction of the turbulence viscosity ratio (Figure 7b) by the SST model in the freestream region diminishes the stratification of temperature (Figure 7a and 8a). However, we show in the subsequent *Flow Regime and Turbulence Model Sensitivity*) section that the laminar and the IDDES approaches fail to overcome this shortcoming of the SST model, which remain the best available choice. Despite its shortcoming in the freestream region, the SST turbulence model seem to perform quite well in the wall-bounded turbulence region including in the thermal boundary layer of the gas interface. Since the laminar and the IDDES model predictions demonstrate similar fluid temperature probe trends as the SST predictions in Figure 8, additional causes such as simplified modeling of the diffuser or any measurement issues in the experiment are also likely responsible for the less stratified temperature field.

Another factor is that - as noted before - the solid walls are modeled with constant thermal properties due to the current solver limitation. While care has been taken to select the constants at a representative temperature for each component, this inherent limitation is expected to result in some time-accurate deviations. Relatedly, the slight under-prediction of the pressurization rate at the low flow rate ($t < 44$ seconds) also owes to higher than actual heat retention by the solid walls because the actual specific heat of these components is lower at these temperatures than the modeled values. Since the solver requires specification of constant properties, the flow regime where the most rapid and consequential pressure changes are occurring was chosen to specify constant properties (Table 3 and 4).

Lastly, under the rapid pressure changes and sharp thermal gradients encountered at the gas liquid interface, quasi-equilibrium is not maintained and the HKS equation prediction may deviate from the actual behavior (see Stewart [13] for a background on the HKS equation 11). Exclusion of the tank man-way plumbing may also introduce small errors due to reduction the thermal mass. A small measurement uncertainty in the experimental data is also possible. The exact location of the diffuser and tank wall temperature probes in Figure 8b are unknown and were estimated from the available schematics.

Some of the trade-offs made in this analysis are often necessary for production problems and the gaps in modeling capabilities must be combined with reasonable understanding of their impact on the predictions. Within the limitations discussed here, the model performs quite well in predicting pressurization of the tank.

A. Mesh Resolution Sensitivity

Mesh independence was ensured by simulating several mesh resolutions, a representative sample of which is shown in Figure 5. All meshes contained enough boundary layer (BL) refinement for the wall integration approach. The pressurization is predicted reasonably well (Figure 10) by all meshes. As noted earlier, using a first cell height smaller than 1×10^{-4} m does not further improve the solution, but it lowers maximum allowable timestep requirement for achieving a time-accurate solution.

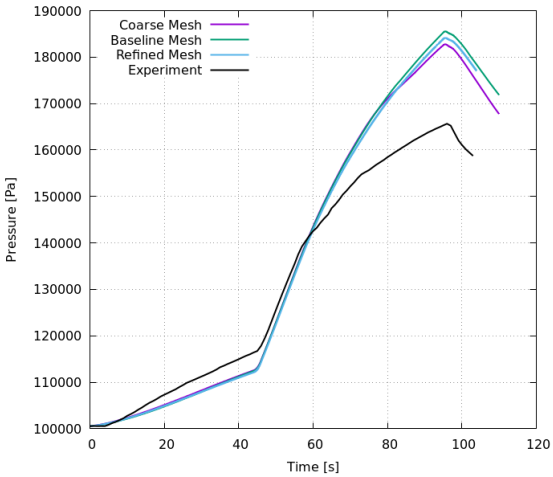

Fig. 10 Mesh Resolution Sensitivity

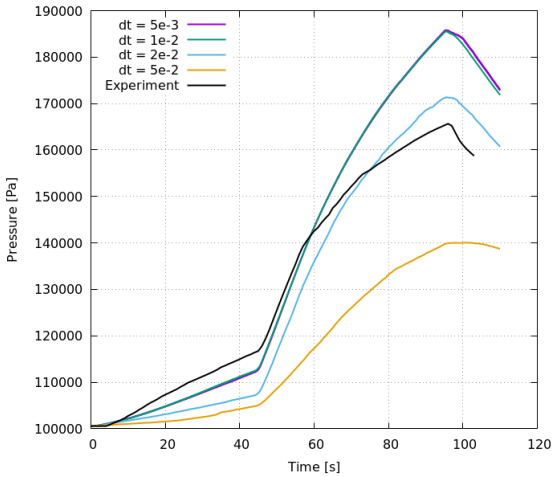

Fig. 11 Timestep Sensitivity

B. Timestep Sensitivity

Loci-Stream employs backward difference schemes for time integration and because these schemes are implicit, the solution is stable even at higher timesteps, but the problem dynamics dictate the maximum allowable timestep that can still resolve the problem in a time-accurate manner. For this problem, the limiting physics for the timestep is resolution of the changing thermal gradient at the interface. We tested timesteps in the range of 1×10^{-4} s to 1×10^{-1} s and found that the maximum allowable timestep reduces for higher mesh resolution at the interface. For the baseline mesh (Figure 5b), a 1×10^{-2} s or lower timestep was necessary for time-accurate solution (Figure 11) but a smaller timestep refinement did not further improve the solution.

C. Flow Regime and Turbulence Model Sensitivity

For turbulence modeling, Menter's SST was compared with the IDDES approach (Figure 12). The laminar flow regime was also compared with these turbulent flow solutions. The laminar approach over-predicts the pressurization compared to the SST turbulence model, while the pressurization predicted by the IDDES approach falls between the predictions of the laminar and the SST model. The laminar and the IDDES flow fields and temperature fields in the ullage are quite similar to the SST solution shown in the Figure 7, but a close inspection shows a warm convective current generated by the diffuser flow traveling around tank wall and reaching the interface without enough mixing with the cold flow like it does in the SST solution. The resultant warmer interface causes higher than expected pressurization. Again, while the SST model has a shortcoming in the freestream region, it is not addressed by the laminar or the IDDES model and the SST model performs better at predicting the turbulence viscosity ratios in the wall-bounded region for resolving the velocity and thermal gradients at the walls and at the interface.

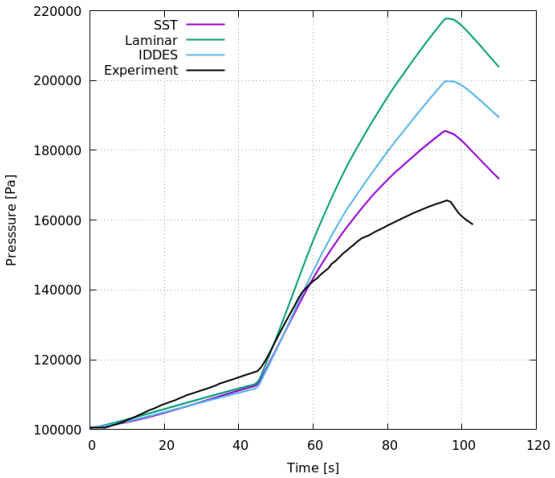

Fig. 12 Sensitivity Flow Regime and Turbulence Model

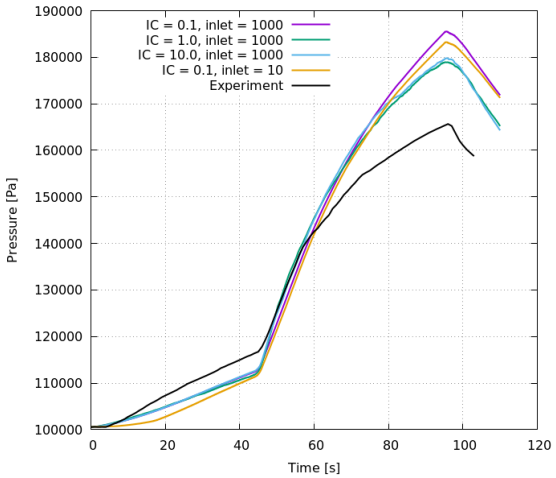

Fig. 13 Sensitivity to Initial and Inlet Turbulence

Sensitivity to the turbulence initial condition (IC) and the inlet turbulence found a modest impact on the pressurization. While inlet turbulence had little effect, higher initial turbulence slightly enhances the prediction (Figure 13).

Sensitivity to the interface boundary turbulence treatment (see section *Turbulence Modeling for Two Phase Interface*) is also assessed (Figure 14). We found that the asymmetric wall-slip approach at the gas-liquid interface performs better than the symmetric wall-wall turbulence boundary approach. The symmetric wall-wall approach performs better when different flow regimes in the tank ullage and liquid are encountered, e.g., self-pressurization with localized heating in a desktop size tank [16] (very low velocity natural convection driven flow on both sides of the interface), axial jet mixing in a flight size tank [17] (high velocities on the liquid side of the interface). More work needs to be done to understand which approach is more suitable for a specific problem.

D. Accommodation Factor Sensitivity

Since the HKS model (Equation 11) for phase change mass transfer has an accommodation factor (AF) that drives the evaporation/condensation rates but does not have an empirically derived value, it is necessary to demonstrate the impact of the AF on the validation of this model. Literature suggests that AF is dependent upon substance and operating

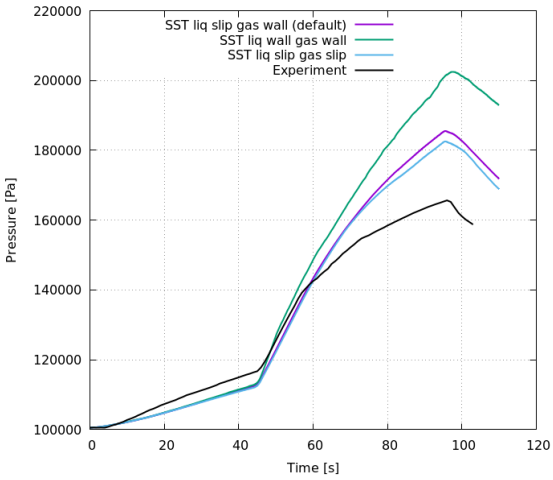

Fig. 14 Sensitivity to Interface Turbulence Boundary Treatment

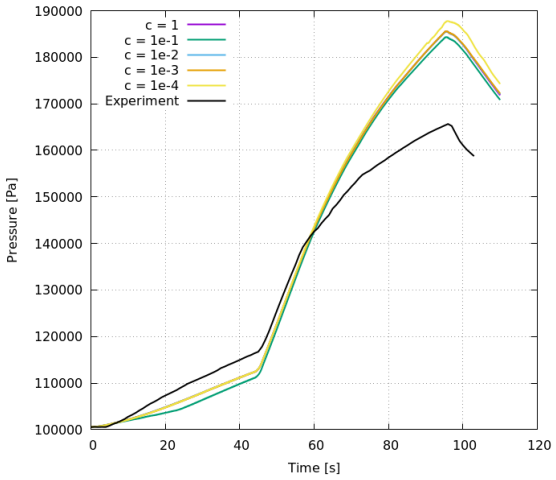

Fig. 15 Accommodation Factor Sensitivity

conditions, though experimentally tested values are difficult to characterize and obtain [8]. We rely on testing model sensitivity to this parameter to avoid model tuning and achieve a generalized model.

In an open system, where the diffuse flow is adding gaseous hydrogen in the constant volume ullage, higher AF is expected to increase the condensation rate. Agreeable to this hypothesis, our assessment found the peak pressure modestly lowers when a higher AF is applied. But an AF larger than 0.1 had no impact on the solution (Figure 15.

VII. Conclusion

Our modeling approach and the Loci-Stream two phase sharp interface CFD model has been validated against the EDU/IVF-100 tank autogenous-pressurization ground experiment. The pressurization prediction compares well with the experiment. A significant portion of the pressurization difference between the experiment and the model is attributable to the ideal gas assumption in the interfacial gas region. The temperature probes comparison shows good prediction at lower diffuser massflow rate but shows diminished thermal stratification due to a known shortcoming of the SST model that over-predicts turbulence conductivity in the ullage. Regardless, the SST model performs well in the wall-bounded region and is perhaps the best choice for an economic, and a robust turbulence model for such problems. Modeling limitations of constant solids thermal properties and latent heat are also identified. Regardless, the most essential flow and thermal dynamics are understood and modeled without any tuning parameters. This practice of simplifying the model to the most salient features not only saves computational resources but also hones engineer's ability to distill important dynamics for problem at hand and is essential for modeling a more complex system. The newly implemented two phase sharp interface module allows at least an order of magnitude higher timestep than VOF would allow, speeding up the computation time at least 10x while also improving the resolution of thermal gradient at the interface, which is an essential problem dynamic.

The validation enhances confidence in our solver's ability to tackle successively more complex CFM problems. In the future, we anticipate implementing a real gas model; implementing temperature-dependent solids properties, and latent heat; exploring opportunities to improve turbulence modeling in the ullage freestream region; and applying the Loci-Stream model to additional autogenous-pressurization problems to further our validation.

Acknowledgments

The NASA High-End Computing (HEC) Program, through the NASA Advanced Supercomputing (NAS) Division at Ames Research Center provided the computational resources for these simulations. We are thankful to Juan Valenzuela (NASA MSFC) for providing access to the EDU tank experimental data and test documentation, and Andre LeClair for helping identify measurement probes used in previous analyses. We are also thankful to our colleagues H. Q. Yang and Jacob Brodnick for helpful discussions.

References

[1] Christian, C., Lehmann, E., and Ruby, L., *Autogenous pressurization for space vehicle propulsion systems*, 1968. https://doi.org/10.2514/6.1968-626, URL https://arc.aiaa.org/doi/abs/10.2514/6.1968-626.

[2] Thakur, S., Wright, J., and Shyy, J. W., "An Algorithm for Chemically Reacting Flows on Generalized Grids Using a Rule-Based Framework," *43rd AIAA Conference*, 2005, p. 0875.

[3] Kamakoti, R., Thakur, S., Wright, J., and Shyy, W., "Validation of a new parallel all-speed CFD code in a rule-based framework for multidisciplinary applications," *36th AIAA Fluid Dynamics Conference and Exhibit, AIAA 2006–3063, San Francisco, CA*, 2006.

[4] Barsi, S., and Kassemi, M., "Investigation of tank pressurization and pressure control part ii: numerical modelling," *ASME J Therm Sci Eng Appl*, Vol. 5, No. 2 [041006], 2013, pp. 1–9.

[5] Barsi, S., and M., K., "Numerical and experimental comparisons of the self-pressurization behavior of an LH2 tank in normal gravity," *Cryogenics*, Vol. 48, No. 3-4, 2008, pp. 122–129.

[6] Schrage, R. W., Columbia University Press, 1953, p. 27.

[7] Linstrom, P., and Mallard, W., "Editors," *NIST Chemistry WebBook, NIST Std. Ref. Database Number 69, NIST*, 2005. URL http://webbook.nist.gov.

[8] Yang, H. Q., Patel, C. S., and Williams, B. R., *Validation of Cryogenic Propellant Tank Self-Pressurization*, 2023. https://doi.org/10.2514/6.2023-1411, URL https://arc.aiaa.org/doi/abs/10.2514/6.2023-1411.

[9] Kassemi, M., Kartuzova, O., and Hylton, S., "Validation of two-phase CFD models for propellant tank self-pressurization: Crossing fluid types, scales, and gravity levels," *Cryogenics*, Vol. 89, 2018, pp. 1–15. https://doi.org/https://doi.org/10.1016/j.cryogenics.2017.10.019, URL https://www.sciencedirect.com/science/article/pii/S0011227517302576.

[10] Frederix, E., Mathur, A., Dovizio, D., Geurts, B., and Komen, E., "Reynolds-averaged modeling of turbulence damping near a large-scale interface in two-phase flow," *Nuclear Engineering and Design*, Vol. 333, 2018, pp. 122–130. https://doi.org/https://doi.org/10.1016/j.nucengdes.2018.04.010, URL https://www.sciencedirect.com/science/article/pii/S0029549318304266.

[11] Egorov, Y., Boucker, M., Martin, A., Pigny, S., Scheuerer, M., and Willemsen, S., "Validation of CFD codes with PTS-relevant test cases," *5th Euratom Framework Programme ECORA project*, Vol. 2004, 2004, pp. 91–116.

[12] Fan, W., and Anglart, H., "Progress in Phenomenological Modeling of Turbulence Damping around a Two-Phase Interface," *Fluids*, Vol. 4, No. 3, 2019. https://doi.org/10.3390/fluids4030136, URL https://www.mdpi.com/2311-5521/4/3/136.

[13] Stewart, M., *Pressurization of a Flightweight, Liquid Hydrogen Tank: Evaporation & Condensation at the Liquid/Vapor Interface*, 2017. https://doi.org/10.2514/6.2017-4916, URL https://arc.aiaa.org/doi/abs/10.2514/6.2017-4916.

[14] Simon, N., Drexler, E., and Reed, R., "Review of Cryogenic Mechanical and Thermal Properties of Al-Li Alloys and Alloy 2219," 1991, pp. 173–178. URL https://nvlpubs.nist.gov/nistpubs/Legacy/IR/nistir3971.pdf.

[15] Kartuzova, O., and Kassemi, M., "Modeling ullage dynamics of tank pressure control experiment during jet mixing in microgravity," *AIAA 52nd joint propulsion conference. Salt Lake City, UT*, 2016.

[16] Patel, C. S., Yang, H. Q., and Williams, B. R., *Validation of Gas-Liquid Sharp Interface Model in Loci-Stream for Propellant Tank Self-pressurization under Normal Gravity*, 2024.

[17] Williams, B. R., Brodnick, J. M., and Reske, E. J., *Validation of a Computational Fluid Dynamics Model of Axial Jet Mixing for Cryogenic Propellant Tank Pressure Control*, 2024.